



Research paper

Preparation and characterization of an amylase-triggered dextrin-linked graphene oxide anticancer drug nanocarrier and its vascular permeability

Siaw Fui Kiew^a, Yan Teck Ho^b, Lik Voon Kiew^{c,*}, James Chen Yong Kah^{b,d}, Hong Boon Lee^a, Toyoko Imae^{e,f}, Lip Yong Chung^{a,*}^a Department of Pharmacy, Faculty of Medicine, University of Malaya, 50603 Kuala Lumpur, Malaysia^b NUS Graduate School for Integrative Sciences and Engineering, National University of Singapore, Centre for Life Sciences (CeLS), #05-01, 28 Medical Drive, 117456, Republic of Singapore^c Department of Pharmacology, Faculty of Medicine, University of Malaya, 50603 Kuala Lumpur, Malaysia^d Department of Biomedical Engineering, National University of Singapore, 4 Engineering Drive 3, Blk E4, #04-08, 117583, Republic of Singapore^e Graduate Institute of Applied Science and Technology, National Taiwan University of Science and Technology, 43 Section 4, Keelung Road, Taipei 10607, Taiwan, ROC^f Department of Chemical Engineering, National Taiwan University of Science and Technology, 43 Section 4, Keelung Road, Taipei 10607, Taiwan, ROC

ARTICLE INFO

Keywords:

Graphene oxide
Dextrin
Triggered release
 α -amylase
Vascular permeability
Microfluidic device

ABSTRACT

We synthesized a dextrin (DEX)-conjugated graphene oxide (GO) nanocarrier (GO₁₀₀-DEX) as a potential drug delivery system to respond to a tumor-associated stimulus, α -amylase, that has high permeability through the fenestrated endothelial barrier to the tumor site. At acidic pH and in the presence of α -amylase to simulate tumor conditions, GO₁₀₀-DEX released a 1.5-fold higher amount of doxorubicin (DOX) than of GO₁₀₀. Under the same conditions, the cytotoxic effects of GO₁₀₀-DEX/DOX were 2-fold greater than those of free DOX and 2.9-fold greater than those of GO₁₀₀/DOX. Employing an *in vitro* biomimetic microfluidic blood vessel model lined with human umbilical vein endothelial cells, we evaluated the tumor vasculature endothelial permeation of GO₁₀₀-DEX and GO₁₀₀ using dextrans of 10 and 70 kDa for comparison and as standards to validate the microfluidic blood vessel model. The results showed that the permeabilities of GO₁₀₀-DEX and GO₁₀₀ were 4.3- and 4.9-fold greater than that of 70 kDa dextran and 2.7- and 3.1-fold higher than that of 10 kDa dextran, thus demonstrating the good permeability of the GO-based nanocarrier through the fenestrated endothelial barrier.

1. Introduction

Nano-sized drug delivery carriers, including polymers, micelles and liposomes, have been extensively explored as nanocarriers to improve the selectivity and targeting of small drug molecules for tumor tissues over healthy tissues (Blum et al., 2015), and some have advanced into clinical stages (Pillai, 2014). Recently, a carbon-based nanomaterial, graphene oxide (GO), has sparked growing interest in the biomedical field owing to its two-dimensional structure, which provides an extremely large surface area (2600 m²/g) and a high drug loading capacity, which is usually above 100 wt% (Siriviriyanun et al., 2015) and is far greater than the loading values of most nanomaterials (Kim et al., 2010; Sun et al., 2008a). GO contains hydrophobic graphenic domains for interacting with water-insoluble drug molecules and hydrophilic edges anchored with carboxyl groups, which give a wide range of chemical functionalization opportunities and good water dispersibility (Kiew et al., 2016).

To improve tumor targeting and selectivity and to reduce the

premature leakage of the drug from the nanocarrier, GO-based nanocarriers have been studied, with the release of their drug cargos being activated by stimuli such as near-infrared light, pH and electricity (He et al., 2014; Kurapati and Raichur, 2013; Weaver et al., 2014). In this study, we seek to develop a GO-based nanocarrier that selectively unloads drugs to tumors with high expression levels of α -amylase (Casadei Gardini et al., 2016; Kawakita et al., 2012; Minami et al., 2014; Shingu et al., 2013; Yanagitani et al., 2007). According to Takeuchi et al. (1981) ovary and lung adenocarcinoma and thymoma show 6.8–15 U/g α -amylase activity, whereas normal tissues have less than 1 U/g of tissue (Lenler-Petersen et al., 1994; Takeuchi et al., 1981). The reason for the overexpression of α -amylase by these tumors remains elusive, but it is conceivable that such overexpression might play a role in the acquisition of nutrients and energy for rapidly growing cancer cells. α -amylase catalyzes polysaccharides into smaller disaccharides optimally at pH 6.7–7.0. Thus, it is expected to function in tumors because the extracellular pH of tumor tissue is between pH 5.8 and 7.6 (Tannock, 1998).

* Corresponding authors.

E-mail addresses: lvkiew@um.edu.my (L.V. Kiew), chungly@hotmail.com (L.Y. Chung).

Employing α -amylase as the tumor-associated stimuli, we conjugated GO (average diameter = 100 nm, GO₁₀₀) with dextran (DEX), a long chain α -1,4-poly(glucose) polymer that is readily degraded by α -amylase, to yield GO₁₀₀-DEX as a stimulus-responsive nanocarrier. The clinical safety of DEX has been well documented. It has been used as a peritoneal dialysis solution, and it has been formulated with 5-fluorouracil for peritoneal administration in cancer treatment (Kerr et al., 1996). We hypothesized that the GO₁₀₀-DEX nanocarrier effectively cages its drug payload within its nanostructure via π - π interactions with the GO surface and physical trapping by the DEX chains. Upon the arrival of the drug-loaded GO₁₀₀-DEX at the tumor site, α -amylase in the tumor interstitium degrades the DEX coating of the GO₁₀₀-DEX, and the trapped drug molecules are released into the tumor microenvironment.

Similar to other nanocarriers, drug delivery by GO₁₀₀-DEX relies on the enhanced permeability and retention effect as a means to passively accumulate at the tumor site. Importantly, for accumulation to occur, the nanocarrier must first be able to permeate through the fenestrated vascular endothelial barrier. To study this, we employed a previously established microfluidic device lined with an endothelial cell monolayer that can approximate cancer endothelial permeability (Ho et al., 2017) to evaluate the permeability of GO₁₀₀-DEX through the endothelial barrier. Our findings suggest that permeability through the vascular endothelial barrier depends on both the size and the shape of the nanocarriers. The 100 nm GO₁₀₀ permeated better than the 130 nm GO₁₀₀-DEX did, and the permeability of these non-spherical GO-based nanocarriers was at least 4.3-fold higher than that of the spherical 70 kDa dextran (Blanco et al., 2015).

This paper is the first study to explore the possibility of using DEX as a surface coating of a GO nanocarrier. DEX acts as the key component in fabricating the GO into a nanocarrier responding to the tumor-associated stimulus α -amylase. This is also the first study to investigate the permeability of GO-based nanocarriers through the vascular endothelial barrier by using a biomimetic microfluidic device to ensure the efficient targeting of this potential nanocarrier to the tumor site.

2. Materials and methods

2.1. Materials and chemicals

Aqueous dispersion of graphene oxide (GO) (4 mg/mL), doxorubicin (DOX), dextran (DEX, corn, type 1), α -amylase (porcine pancreases, Type VI-B), *N*-(3-dimethylampropyl)-*N*'-ethylcarbodiimide hydrochloride (EDC), fibrinogen, thrombin and fibronectin were purchased from Sigma-Aldrich, USA. Hydrochloric acid (37%) and sodium hydroxide were from Fisher Chemical, UK. Sodium bicarbonate (NaHCO₃) and acetonitrile (ACN) were supplied by Merck, Germany and ACROS, USA, respectively. Pullulan standards (MW, 6 & 12 kDa) for gel permeation chromatography (GPC) analysis were purchased from Fluka, Germany. Dialysis tubing (MWCO 3500 Da) were from Fisher Scientific, USA. Fetal bovine serum (FBS) and RPMI medium 1640 (1 ×) supplemented with L-glutamine were purchased from GIBCO, Brazil. Endothelial growth medium (EGM-2) and human umbilical vein endothelial cells (HUVECs) were supplied by Lonza, Switzerland. Oregon Green 488-tagged 10 kDa and Texas Red-tagged 70 kDa dextrans were purchased from Life Technologies, USA, and rhodamine and sulfo-*N*-hydroxysulfosuccinimide (NHS) were from Thermo Fisher Scientific, USA. 4T1 (murine breast carcinoma) cells were supplied by ATCC, USA. Sterilized ultrapure water with a resistivity of 18.2 M Ω .cm (ELGA, UK) was used for all synthesis, characterization and evaluation.

2.2. Preparation of GO₁₀₀ nanocarrier

To prepare GO₁₀₀ (100 nm), 5 μ m GO sheets were fractured via ultrasonication for several hours using an ultrasonic processor equipped with a standard probe with a tip diameter of 19 mm (Sonics & Materials,

VCX 400), with the amplitude intensity set at 25% and power at 40 W (Siriviriyannun et al., 2015). Throughout the ultrasonication process, the sample was kept in an ice-bath for heat dissipation. The sonicated GO was then filtered through a cellulose acetate membrane with a pore size of 0.2 μ m to remove oversized GO sheets. A smaller pore size (e.g., 0.1 μ m) was not used due to clogging and excessive sample loss. The size of the filtered GO dispersion was determined using a Malvern Zetasizer (Nano ZSP, Worcestershire, UK). The ultrasonication and filtration processes were repeated until the size of the GO sheets was reduced to 100 nm.

2.3. Preparation of low molecular-weight dextrin

Low molecular weight DEX was prepared by a simple and facile method: filtration of the dextrin aqueous (8 mg/mL) solution through a series of cellulose acetate membranes with pore sizes of 0.2, 0.1 and 0.02 μ m to gradually reduce the molecular weight. The molecular weight of the resultant DEX was characterized by gel permeation chromatography (GPC; Agilent GPC 1260 Infinity Multi-Detector Suite assembled with viscometer, refractive index, dual angle light scattering and various wavelength detectors, USA) equipped with 7.8 × 300 mm Ultrahydrogel™ Linear columns (Waters, Japan). Water was used as the eluent at a flow rate of 0.6 mL/min. Pullulans (MW, 6 and 12 kDa) were used as standard references because they have similar chemical structures and functional groups as DEX does.

2.4. Preparation of GO₁₀₀-DEX, GO₁₀₀/DOX and GO₁₀₀-DEX/DOX

Dextrin-conjugated graphene oxide (GO₁₀₀-DEX) was synthesized by a modified esterification process in water-containing solvent as shown in Fig. 1(a) (Wang et al., 2012), using EDC as the coupling agent to chemically conjugate the DEX to GO₁₀₀. The process began with 30 min of bath sonication of GO₁₀₀ (400 μ g/mL, 4 mL) and DEX (32 μ g/mL, 4 mL) separately to ensure the even dispersion of the samples. The GO₁₀₀ was vigorously stirred using a magnetic stirrer for 15 min before adding NaHCO₃ (0.4 g), ACN (200 μ L, 0.2 M) and EDC (0.2 g). After another 15 min of stirring, DEX was added. The mixture was further stirred for 5.5 h at 0 °C to allow the esterification reaction to occur. At the end of the reaction, the mixture was centrifuged three times at 16000 × g with ultrapure water to remove the excess unreacted reagents. GO₁₀₀-DEX was collected and redispersed in ultrapure water, and the concentration was determined by the absorbance at 230 nm using a standard calibration curve plotted with absorbance of GO dispersions of known concentrations, 0–25 μ g/mL. The presence of DEX did not affect the concentration determination of GO₁₀₀-DEX because its absorbance at this wavelength is negligible.

To load DOX onto GO₁₀₀ and GO₁₀₀-DEX, GO₁₀₀ (2 mL, 100 μ g/mL) and GO₁₀₀-DEX (2 mL, equivalent to 100 μ g/mL of GO) were separately mixed with an aqueous solution of DOX (2 mL, 200 μ g/mL; Fig. 1(b)). Both single-sheet surfaces of the two-dimensional GO are accessible for drug interaction. Because a drug loading rate of 235 wt% has been reported for GO nanocarrier (Yang et al., 2008), 2 mL of DOX at a concentration of 200 μ g/mL was loaded onto 2 mL of GO nanocarriers at a concentration of 100 μ g/mL. The mixture was stirred for 24 h in the dark before being washed twice with ultrapure water by centrifugation at 16000 × g for 1 h to remove the unbound DOX. Finally, GO₁₀₀/DOX and GO₁₀₀-DEX/DOX dispersions were made by resuspension of the pellet.

The absorbance value of the unbound DOX remaining in the supernatant was measured using a UV-vis spectrophotometer at a wavelength of 480 nm. The DOX loading (% w/w) was calculated based on the formula below (Siriviriyannun et al., 2015):

$$\text{Drug loading (\%w/w)} = ((M_{\text{DOX}} - M_{\text{DOX}}^*)/M_{\text{GO}}) \times 100$$

where M_{DOX} is the initial amount of DOX, M_{DOX}^* is the total amount of

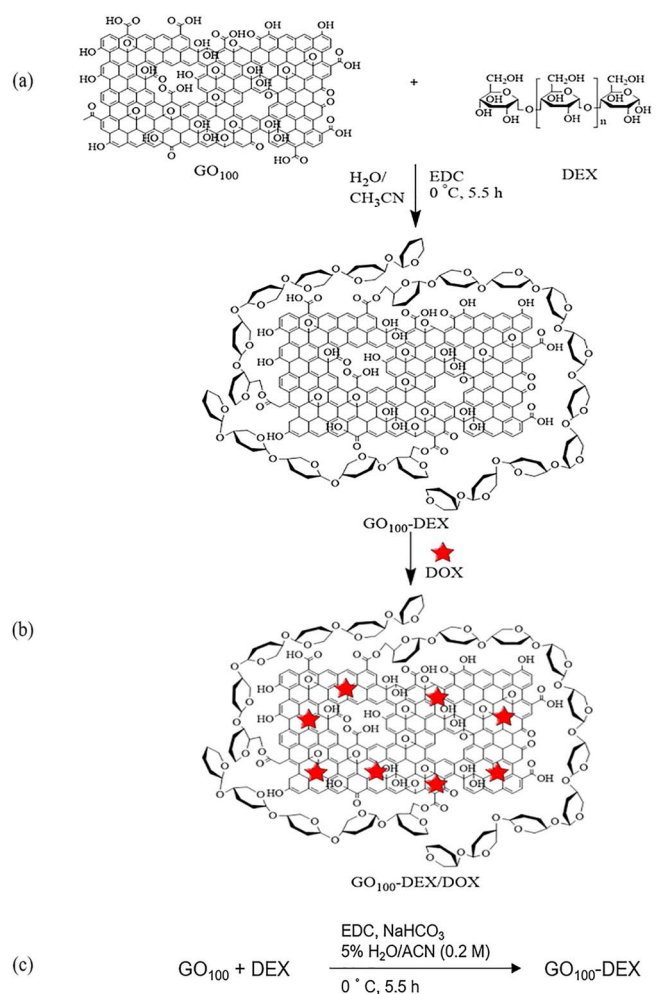


Fig. 1. (a) Conjugation reaction of GO₁₀₀ and DEX to form GO₁₀₀-DEX. (b) Loading of DOX onto GO₁₀₀ and GO₁₀₀-DEX. (c) Reaction equation for GO₁₀₀-DEX synthesis.

unbound DOX and M_{GO} is the amount of GO₁₀₀ or GO₁₀₀-DEX.

2.5. Characterization of GO₁₀₀ and GO₁₀₀-DEX nanocarriers

The hydrodynamic diameter (D_H), size distribution and zeta potential of GO₁₀₀ and GO₁₀₀-DEX were measured using a zetasizer based on the principles of dynamic light scattering and electrophoresis. The physical properties and functional groups of the GO₁₀₀, DEX and GO₁₀₀-DEX were characterized using UV-Vis, infrared (IR) and Raman spectrometers. The thermal stability of the samples was analyzed by thermogravimetric analysis (TGA) at a 10 °C/min heating rate.

The surface morphologies of the samples were obtained by transmission electron microscope (TEM; LEO LIBRA-120), and the thickness of the samples was measured by atomic force microscopy (AFM) using a Digital Instrument NanoScope III.

2.6. *In vitro* drug release of GO₁₀₀/DOX and GO₁₀₀-DEX/DOX at pH 7.4 and pH 5.8 and in the presence or absence of α -amylase

Investigation of the *in vitro* DOX release was carried out at pH 7.4 and pH 5.8 in the absence or presence of α -amylase to simulate the physiological tumor environment (Yang et al., 2008). First, 2 mL samples of GO₁₀₀/DOX and GO₁₀₀-DEX/DOX containing 100 μ g/mL of DOX were each equally divided into 4 tubes. Then, 2 tubes for each sample were mixed with 1 mL PBS containing 6 unit/mL of α -amylase, and the remaining tubes were mixed with 1 mL PBS. The use of 6 unit/mL of α -amylase was based on the average amylase activity of tumor tissues

obtained from 10 patients reported in a previous study (Lenler-Petersen et al., 1994). The samples were pipetted into dialysis bags (MWCO 3500) and then immersed in 10 mL of PBS solution at pH 7.4 and pH 5.8 (Feng et al., 2014), at 37 °C with orbital shaking at 100 rpm. At specific time points from 0 to 48 h, 1 mL of PBS solution (release medium) was sampled from each test sample and an equal volume of fresh PBS was added. The absorbance values of the released DOX from three independent experiments were measured in triplicate using a UV-vis spectrophotometer at a wavelength of 480 nm.

2.7. *In vitro* cytotoxicity of GO₁₀₀/DOX and GO₁₀₀-DEX/DOX at pH 7.4 and pH 6.6 and in the presence of α -amylase, and their cell compatibility and hemocompatibility

The cytotoxicity of free DOX, GO₁₀₀/DOX and GO₁₀₀-DEX/DOX was evaluated in two different conditions: (i) pH 7.4 to represent a healthy tissue microenvironment and (ii) pH 6.6 and in the presence of α -amylase to simulate tumor conditions. Instead of pH 5.8, pH 6.6 was used in the cytotoxicity study because most cells cannot proliferate at a pH lower than 6.6 (Tannock, 1998). 4T1 cells at 5000 cell/well were seeded in 96-well plates and allowed to grow overnight. For condition (i), the RPMI medium in the 96-well plate was replaced with fresh RPMI medium without any pH changes. For condition (ii), the medium was replaced with fresh RPMI medium with its pH adjusted to 6.6 by 1 N HCl (Gerweck et al., 1999) combined with 10 μ L of 6 unit/mL α -amylase in PBS. The cells were treated with free DOX, GO₁₀₀/DOX and GO₁₀₀-DEX/DOX with concentrations ranging from 0 to 20 μ g/mL (equivalent to concentration of DOX). After incubation (24 h or 48 h), MTT solution (5 mg/mL in PBS) was added and the formazan formed was dissolved in DMSO. Absorbance values of the solution from three independent experiments were read in triplicate at a wavelength of 570 nm, and the percentage of cell viability was calculated based on the formula below:

$$\text{Percentage of cell viability} = (\text{OD treated}/\text{OD control}) \times 100$$

The cell compatibility and hemocompatibility of GO₁₀₀ and GO₁₀₀-DEX and their DOX-loaded derivatives were conducted using methods similar to those described in a previous study (Liao et al., 2011). For details, refer to the Supporting information.

2.8. Intracellular localization of DOX, GO₁₀₀/DOX and GO₁₀₀-DEX/DOX at pH 7.4 and pH 6.6 and in the presence of α -amylase

The intracellular localization of DOX, GO₁₀₀/DOX and GO₁₀₀-DEX/DOX was studied by confocal microscopy using a dual staining technique, similar to a previous study (Viswanathan et al., 2016). For details, refer to the Supporting information.

2.9. Vascular permeability study of GO₁₀₀ and GO₁₀₀-DEX using a biomimetic microfluidic blood vessel model lined with a fenestrated HUVECs monolayer

The microfluidic devices (Fig. S1) were made from polydimethylsiloxane (PDMS) substrate using a standard soft lithography technique (Tang and George, 2010) reported in a previous study (Ho et al., 2017). To mimic the extracellular matrix, 7 μ L of fibrin solution (5 mg/mL fibrinogen: 1.24 units/mL thrombin = 1:1) was added to the device through port 7 and was allowed to polymerize at 37 °C for 30 min to form a gel. Before cell seeding, the endothelial channel was incubated with 50 μ g/mL fibronectin from human plasma dissolved in EGM-2 culture medium for 1 h at 37 °C and 5% CO₂ to provide a conducive surface for HUVEC attachment. Then, 30 μ L of well-mixed HUVEC cell suspension at a concentration of 10×10^6 cells/mL was pipetted into the ultraviolet-sterilized microfluidic devices through port 1. The devices were incubated at 37 °C with 5% CO₂ for 4 h to allow cell

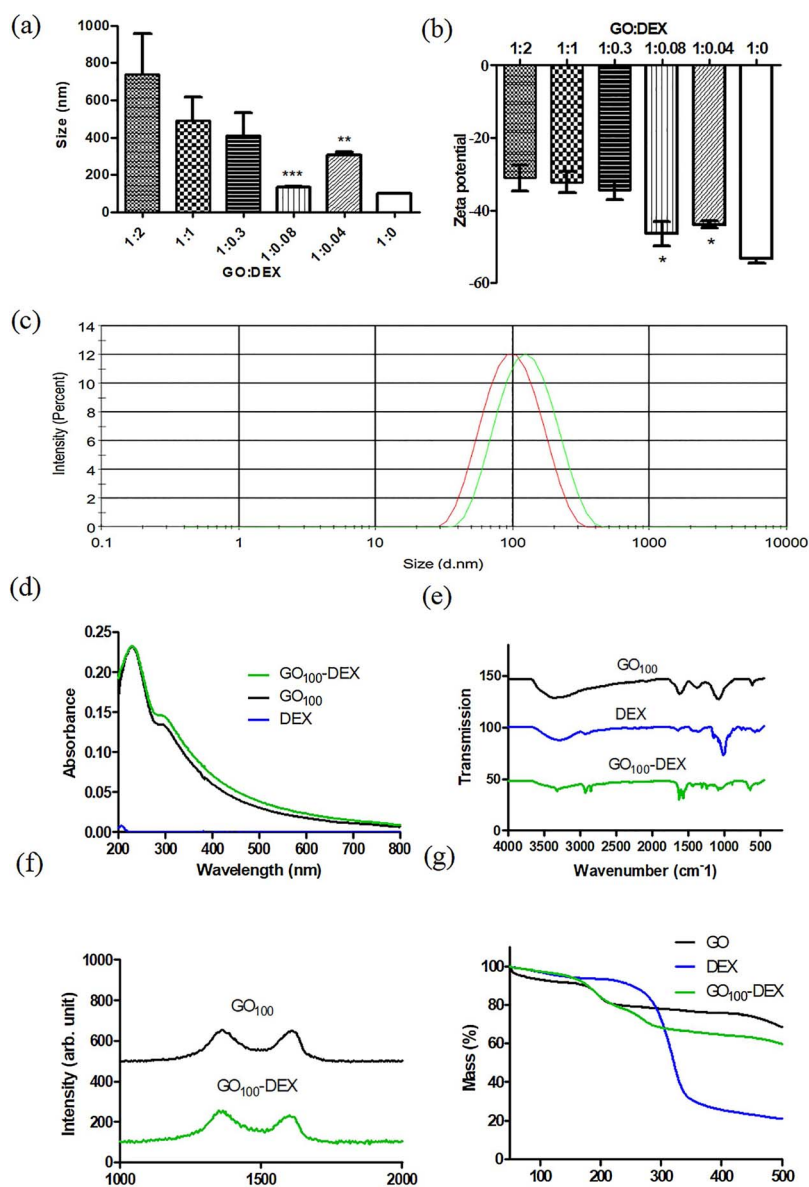


Fig. 2. (a) Size and (b) zeta potential measurements of different formulations of GO₁₀₀-DEX (Data represent mean \pm SEM (n = 3)). (c) Size distribution of GO₁₀₀ (red line) and GO₁₀₀-DEX (green line). (d) UV-vis spectra, (e) Fourier transform infrared (FTIR) absorption spectra, (f) Raman spectra and (g) Thermogravimetric analysis (TGA) of GO₁₀₀, DEX and GO₁₀₀-DEX. (For interpretation of the references to colour in this figure legend, the reader is referred to the web version of this article.)

attachment. The EGM-2 was changed every 24 h for 5 days until a fully confluent endothelial monolayer had formed on the internal surface of the devices. To validate the biomimetic microfluidic blood vessel model, Oregon Green 488-tagged 10 kDa ($\lambda_{ex}/\lambda_{em}$ = 501/526 nm) and Texas Red-tagged 70 kDa dextrans ($\lambda_{ex}/\lambda_{em}$ = 561/594 nm) were used. The dextrans were also used as the comparator groups to study the vascular permeability of the GO nanocarriers.

To tag fluorescent labels to the GO nanocarriers, the $-COOH$ groups on the GO domains of GO₁₀₀ and GO₁₀₀-DEX were conjugated with rhodamine ($\lambda_{ex}/\lambda_{em}$ = 557/576 nm) via an amidation reaction (Konkena and Vasudevan, 2012). Briefly, GO₁₀₀ or GO₁₀₀-DEX (250 μ g/mL) was mixed with a freshly prepared aqueous solution containing EDC and NHS. The mixture was stirred for 10 min and sonicated for 1 min before rhodamine (5 μ g/mL) was added. The mixture was further stirred for 1 h at room temperature. The rhodamine-conjugated GO₁₀₀ and GO₁₀₀-DEX were dialyzed overnight against a tris(hydroxyl)aminomethane solution at 4 $^{\circ}$ C to remove the excess rhodamine. The emission intensities of GO₁₀₀-rhodamine and GO₁₀₀-DEX-rhodamine were determined at an excitation wavelength of 540 nm. There was less than 5% difference in their emission intensities, suggesting that a similar amount of rhodamine was conjugated onto both GO-based nanocarriers.

Fifteen microliters of the fluorescently tagged dextrans GO₁₀₀ and GO₁₀₀-DEX were added to the microfluidic devices through port 1 and allowed to completely fill the HUVEC-lined endothelial channel. Then, time lapse images were acquired at intervals of 30 s for 45 min to observe the diffusion of fluorescent material across the endothelial barrier into the gel region. Images of the sample distribution were taken using a fluorescence microscope (Olympus IX-81, Andor's iXon EMCCD camera; Olympus, Tokyo, Japan). The captured images were then analyzed using MATLAB to calculate the fluorescence intensity across the monolayer with a previously reported method (Ho et al., 2017) (Fig. S2). The diffusional permeability (P_d) was calculated from the captured fluorescence images based on the following equation (Ho et al., 2017).

$$P_d = \frac{1}{(I_{lumen} - I_{gel})_{@t=0}} \times \left(\frac{dl}{dt} \right)_{gel @ t=0} \times \frac{A_{gel}}{W_{manolayer}}$$

where I_{lumen} is the average fluorescence intensity of the lumen of the HUVEC channel (demarcated as yellow ROIs) and I_{gel} is the average local intensity one pixel wide within the gel adjacent to the HUVEC monolayer (indicated by the blue ROI), both at time = 0; $\left(\frac{dl}{dt} \right)$ is the rate of change of average fluorescence intensity within the red ROI at time $t=0$; A_{gel} refers to the surface area of the red ROI within the gel;

and Wmonolayer is the width of the HUVEC monolayer across which diffusion occurs. Figure S3 shows representative fluorescent images at $t = 0$ min and at $t = 30$ min of dextrans, GO₁₀₀ and GO₁₀₀-DEX.

2.10. Statistical analysis

All experimental results were statistically analyzed by Student's *t*-test in GraphPad Prism 5 to compare the analyzed samples. * denotes statistical significance (* for $p \leq 0.05$, ** for $p \leq 0.001$ and *** for $p \leq 0.0001$) vs the control.

3. Results and discussion

3.1. Preparation and characterization of GO₁₀₀ and GO₁₀₀-DEX

We produced GO₁₀₀ and GO₁₀₀-DEX at controlled sizes from 100 to 200 nm because most liposome and viral vectors designed for therapeutic uses have sizes from 100 to 300 nm (Liu and Auguste, 2015). Furthermore, Liu et al. (1992) reported that liposomes with sizes in the range of 100–200 nm were 4-fold more abundant in tumors than were liposomes with sizes below 50 nm or above 300 nm (Liu et al., 1992).

GO₁₀₀, with a zeta potential of -55 mV, was fragmented from 5 μ m GO sheets, and DEX was prepared by the simple filtration of commercial DEX dissolved in ultrapure water through a series of cellulose acetate membrane filters. This simple filtration method is practical and useful, as tedious multiple steps involving multiple reagents and reaction times (Chen et al., 2011) will increase the production cost and the acidic hydrolysis (Tømmeraaas et al., 2001) process may result in cytotoxic products.

We formulated several GO₁₀₀-DEX conjugates by varying the amount of DEX to react with GO₁₀₀ (Fig. 2(a)) using an optimized esterification method in water-containing solvent systems, as shown in Fig. 1(a) (Wang et al., 2012). The rationale of using water-containing solvent systems instead of an organic-based system is to prevent the aggregation of the resultant GO₁₀₀-DEX. The ratio of sample concentrations in the reactions was used to designate the different GO₁₀₀-DEX formulations. For example, a ratio of 1:0.08 indicates 1 mg/mL of GO₁₀₀ conjugated with 0.08 mg/mL of DEX.

GO₁₀₀-DEX at a ratio of 1:0.08 had a size of 133 ± 7.18 nm (Fig. 2(a)), which fulfilled the size requirement as a nanocarrier for potentially higher accumulation in tumor tissue (Liu et al., 1992), whereas the other formulations were larger than 200 nm. This ratio also had the highest negative zeta potential value (-44 mV; Fig. 2(b)), which indicated that it had better water dispersibility compared to other formulations. Thus, GO₁₀₀-DEX at the ratio of 1:0.08 was selected as the drug delivery system in this study. Fig. 2(c) shows the size distribution of GO₁₀₀ (red line) and GO₁₀₀-DEX (green line). The dextrin conjugation caused a 30 nm shift (GO₁₀₀ is 100 nm and GO₁₀₀-DEX is 130 nm) of the size distribution, indicating a homogeneous increase in the size of the resultant conjugated GO₁₀₀-DEX.

In the UV–vis spectra, GO₁₀₀ showed a characteristic absorption band at 230 nm ($\pi \rightarrow \pi^*$) for C=C and a shoulder peak at 300 nm ($n \rightarrow \pi^*$) corresponding to C=O (Sun et al., 2008a; Fig. 2(d)). GO₁₀₀-DEX showed a similar absorption pattern to GO₁₀₀, with a slight increase in the 300 to 600 nm range, probably due to the DEX conjugation increasing both the π -plasmon of carbon and the absorbance of GO₁₀₀-DEX in the visible range (Zhang et al., 2011).

The IR spectrum (Fig. 2(e)) showed that GO₁₀₀ gave a band at approximately 1622 cm^{-1} due to C=C bonds, along with a stretching vibration band of O–H groups at 3363 cm^{-1} . DEX showed bands at approximately 2889 cm^{-1} and 3400 cm^{-1} , which were attributed to C–H bonds and O–H groups, respectively (Predoi, 2007). GO₁₀₀-DEX gave two bands at approximately 2851 and 2926 cm^{-1} due to the presence of C–H groups in the DEX chain that were not found in GO₁₀₀. GO₁₀₀-DEX also contained one band at 1625 cm^{-1} , which was not found in DEX for the C=C bonds of GO₁₀₀. The characteristic carbon

bands in the Raman spectrum are located at approximately 1600 and 1300 cm^{-1} , corresponding to the graphite (G-band) and diamondoid bands (D-band), respectively (Fig. 2(f)).

The weight loss of GO₁₀₀ at approximately 100 °C was approximately 8% and an additional of 13% at 225 °C (Fig. 2(g)). The former weight loss was due to the evaporation of adsorbed water and the latter was due to the decomposition of labile oxygen-containing functional groups on GO₁₀₀ (Bao et al., 2011). DEX showed a major weight loss (60%) at 300 – 400 °C, probably due to the degradation of the DEX backbone (Kim et al., 2011). GO₁₀₀-DEX was also observed to lose 10% more weight at 350 – 450 °C than GO₁₀₀ did. This result suggests that GO₁₀₀-DEX is composed of 10% of DEX and 90% of GO.

In the TEM images (Fig. S4), GO₁₀₀ appeared as transparent nano-sized planar sheets, whereas GO₁₀₀-DEX had a slightly lower transparency due to the DEX coating. The edge functionalization was barely visible in TEM images. However, by AFM, the thickness of GO₁₀₀ was increased from 1.5 nm (Kuila et al., 2012) to approximately 6 nm after coating with DEX.

3.2. Drug loading and drug release of GO₁₀₀ and GO₁₀₀-DEX at different pH values in the presence or absence of α -amylase

GO₁₀₀-DEX was found to have high drug (DOX) loading capacity (~ 180 wt%, ~ 360 μ g of DOX loaded onto 200 μ g of GO₁₀₀-DEX) (Fig. 3(a)), similar to GO₁₀₀. Drug loading onto the GO nanocarrier is mainly mediated by π - π stacking and hydrogen bonding between DOX and GO₁₀₀ (Yang et al., 2008). The similar drug loading capacities of GO₁₀₀-DEX and GO₁₀₀ suggested that the covalent conjugation of DEX did not significantly compromise the loading capacity of GO ($p > 0.05$). However, it is conceivable that some DOX molecules might have been trapped by or interacted with the DEX chains that were covalently linked to GO. The 64% drug loading capacity of GO₁₀₀ and GO₁₀₀-DEX is 6-fold higher than polymer micelles and liposomes, for which the loading capacities are usually approximately 10% based on the equation below (Kim et al., 2010; Sun et al., 2008b). Therefore, the high drug loading capacity of GO₁₀₀-DEX may reduce dosing frequency.

Drug loading

$$= \frac{\text{Mass of drug}}{\text{Total mass of drug + micelle / liposome / GO}_{100} / \text{GO}_{100} - \text{DEX}} \times 100\%$$

The drug release profile of GO₁₀₀/DOX and GO₁₀₀-DEX/DOX was studied in conditions simulating healthy tissue (pH 7.4) and the tumor microenvironment (pH 5.8 and α -amylase) (Tannock, 1998). At pH 5.8 in the presence of α -amylase, we found that GO₁₀₀-DEX released 48% of bound DOX after 48 h, which was 1.5-fold higher than that of GO₁₀₀ under the same conditions (Fig. 3(c)(i)). Without α -amylase (Fig. 3(c)(ii)), GO₁₀₀-DEX released approximately 28% of bound DOX, similar to the values obtained for GO₁₀₀. At pH 7.4, GO₁₀₀ and GO₁₀₀-DEX released approximately 20% of the bound DOX, similar to the results of a previous study (Sun et al., 2008b). GO₁₀₀ and GO₁₀₀-DEX released more DOX in acidic pH due to the protonation of the amino group of DOX molecule ($\text{pK}_a = 8.3$), which weakens its interaction with GO nanocarriers (Yang et al., 2008). At pH 7.4, a high fraction of uncharged DOX molecules exists and forms more hydrogen bonds with GO, resulting in less DOX release (Yang et al., 2008). This may reduce the toxic effects of DOX on normal healthy tissues (pH 7.4).

To understand the release mechanism of DOX from GO₁₀₀/DOX and GO₁₀₀-DEX/DOX, the drug-loaded GO₁₀₀ and GO₁₀₀-DEX release profiles (Fig. 3(c)(i) and (ii)) were fitted into several models, including zero order, first order, Higuchi, Korsmeyer-Peppas and Hixson-Crowell (Matthaiou et al., 2014). Table 1 shows that the R^2 values for Higuchi were generally higher than other kinetic models, suggesting that the release of DOX occurred through a diffusion mechanism.

As DEX is readily degraded by α -amylase into smaller fragments

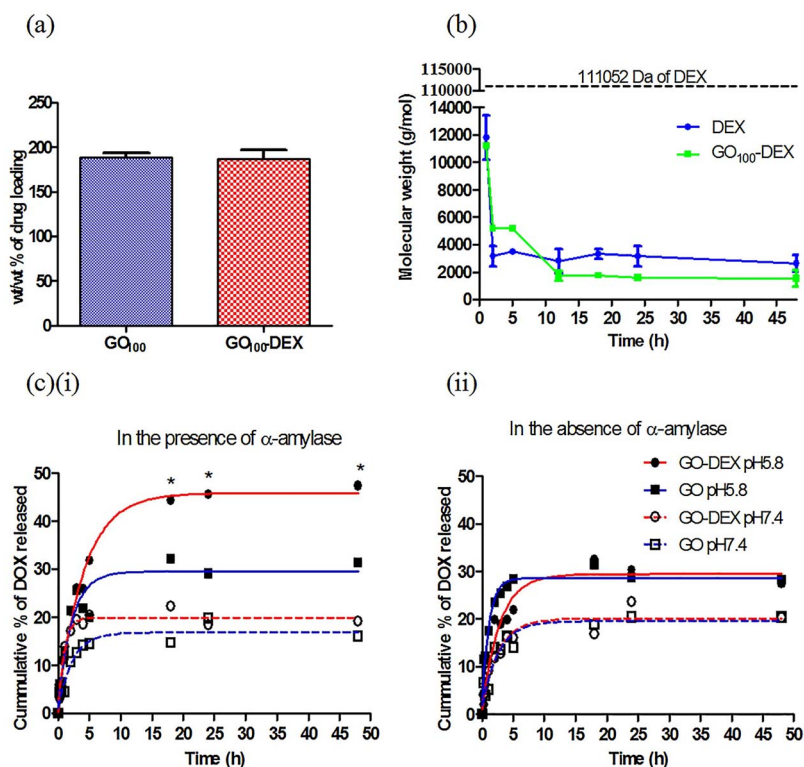


Fig. 3. (a) wt/wt% of GO₁₀₀ and GO₁₀₀-DEX drug loading, (b) degradation of DEX and GO₁₀₀-DEX by α-amylase. The dashed line indicates the initial molecular weight of DEX. Drug release study (c) of GO₁₀₀/DOX and GO₁₀₀-DEX/DOX (i) in the presence (ii) and absence of α-amylase at pH 7.4 and pH 5.8 (Data represent mean ± SEM (n = 3)).

(Hreczuk-Hirst et al., 2001), we postulated that the higher amount of DOX release from GO₁₀₀-DEX in the presence of α-amylase was due to enzymatic degradation of the DEX coating that physically trapped the DOX molecules. Therefore, we examined this hypothesis by investigating the degradation rate of GO₁₀₀-DEX and DEX treated with α-amylase (Fig. 3(b)) over the same durations of time implemented in the drug release study. The degradation of DEX was corroborated by a reduction in molecular weight as measured by a GPC instrument. The results showed that the initial molecular weight of DEX decreased by 85–90% after 1 h of incubation with α-amylase at 37 °C (Hreczuk-Hirst et al., 2001). The rapid initial hydrolysis produced fragments of molecular weights around 10,000–13,000 Da within 1 h. Then, the degradation rate slowed from the fifth hour up to 48 h. The DEX degradation rate explains the higher release rate of DOX from GO₁₀₀-DEX in the first 5 h (Fig. 3(c)(i)), and the release rate slows as the DEX degradation rate slows. This result implies that DOX molecules trapped in

DEX chains were released when DEX was degraded by α-amylase.

3.3. Cytotoxicity, hemocompatibility and intracellular location of DOX, GO₁₀₀/DOX and GO₁₀₀-DEX/DOX at different pH values in the presence or absence of α-amylase

The cytotoxicity of free DOX, GO₁₀₀/DOX and GO₁₀₀-DEX/DOX was studied in different extracellular microenvironments, (i) pH 7.4 to represent a healthy tissue microenvironment, and (ii) pH 6.6 and in the presence of α-amylase to simulate tumor conditions. At pH 7.4, free DOX had the highest cytotoxicity (IC₅₀ = 1.89 μg/mL), followed by GO₁₀₀-DEX/DOX (8.01 μg/mL) and GO₁₀₀/DOX (11.71 μg/mL) after 24 h of treatment (Fig. 4(a)). This was probably because only 20% of DOX was released from GO₁₀₀ and GO₁₀₀-DEX at 24 h, as shown in the release study (Fig. 3(c)(ii)). The GO₁₀₀-DEX/DOX and GO₁₀₀/DOX had at least 4.2-fold lower toxicity (p < 0.05) compared to free DOX. This

Table 1

Release kinetic analysis. M_t is the amount of drug release at time t , $\frac{M_t}{M_\infty}$ is the fraction of drug release at time t , k is the rate constant and \log is natural logarithm.

Kinetic Model (Equation)	Coefficients of correlation (R ²)							
	GO ₁₀₀ -DEX/DOX				GO ₁₀₀ /DOX			
	In the presence of α-amylase		In the absence of α-amylase		In the presence of α-amylase		In the absence of α-amylase	
	pH 5.8	pH 7.4	pH 5.8	pH 7.4	pH 5.8	pH 7.4	pH 5.8	pH 7.4
Zero Order ($M_t = kt$)	0.904	0.766	0.809	0.874	0.681	0.893	0.782	0.755
First Order ($\log(1 - M_t) = -kt$)	0.926	0.782	0.822	0.887	0.678	0.903	0.818	0.761
Higuchi ($M_t = k\sqrt{t}$)	0.967	0.926	0.926	0.975	0.972	0.959	0.949	0.889
Korsmeyer-Peppas ($\frac{M_t}{M_\infty} = kt^n$)	0.898	0.910	0.894	0.953	0.876	0.876	0.969	0.688
Hixson-Crowell ($1 - \sqrt[3]{1 - M_t} = k_{1/3}t$)	0.919	0.777	0.919	0.882	0.679	0.899	0.806	0.759

The values in bold represent relatively higher R2 values.

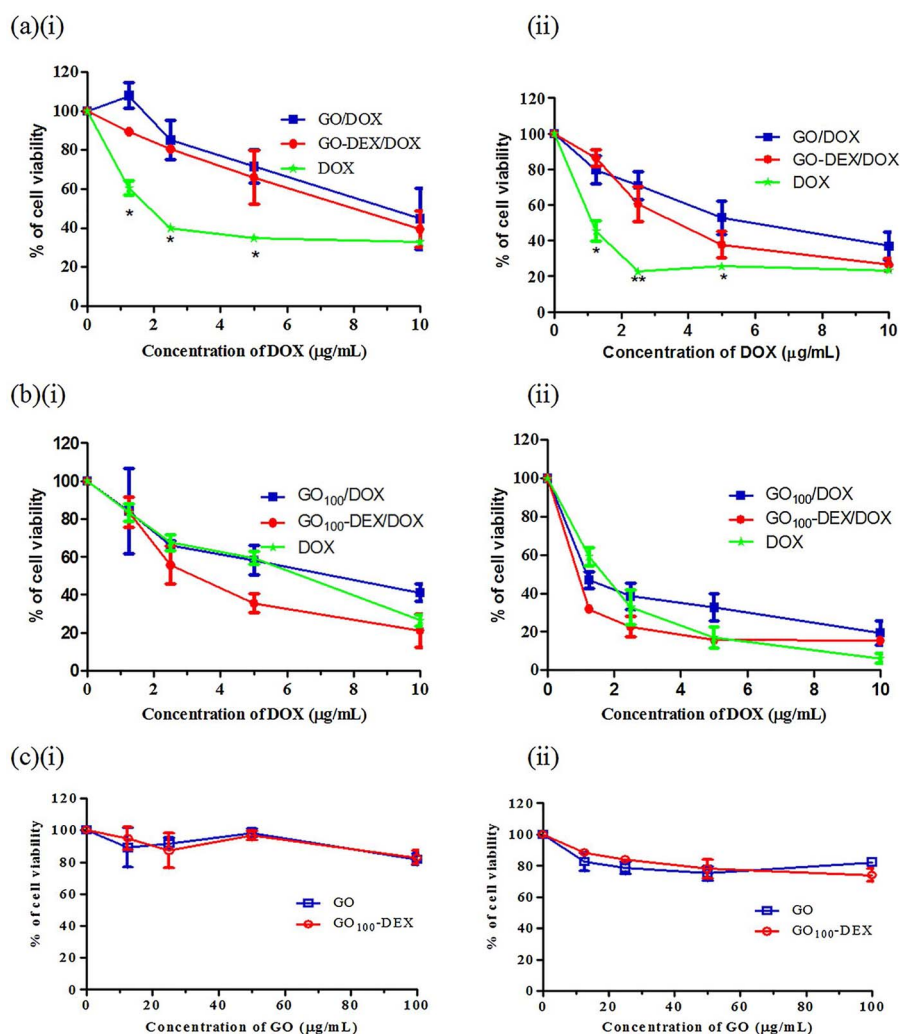


Fig. 4. Cytotoxicity of free DOX, GO₁₀₀/DOX and GO₁₀₀-DEX/DOX on 4T1 cells (a) at pH 7.4 and (b) pH 6.6 and in the presence of α -amylase after (i) 24 h and (ii) 48 h treatment. (c) Cell compatibility of GO₁₀₀ and GO₁₀₀-DEX in 4T1 cells at (i) 24 h and (ii) 48 h (Data represent mean \pm SEM (n = 3)).

result indicates that GO₁₀₀-DEX and GO₁₀₀ can significantly reduce the toxicity of free DOX for cells in the microenvironment of normal tissue. A similar trend was observed for the 48-h treatment.

To simulate tumor conditions, we adjusted the pH of the culture medium to 6.6 (Tannock, 1998) and added 6 unit/mL of porcine α -amylase based on the level of amylase activity reported in cancer tissues (Takeuchi et al., 1981). The cytotoxicity of free DOX was significantly reduced by 3.4-fold (IC_{50} = 6.44 μ g/mL; Fig. 4(b)) compared to that in a healthy tissue microenvironment (1.89 μ g/mL; Fig. 4(a)). This is because the weakly basic DOX (pKa = 8.3) is ionized at acidic pH and possibly trapped in the extracellular compartment (Mahoney et al., 2003; Tannock, 1998). Ionized DOX is not completely membrane-impermeable but has a slower diffusion rate into the cell nucleus, where it causes toxicity (Swietach et al., 2012). These explanations are supported by the results of the intracellular localization study, where we observed that at pH 7.4, majority of free DOX was localized inside the nucleus (Fig. 5(a)) (El-Kareh and Secomb, 2005). In the tumor-mimicking condition, however, we observed that the distribution of free DOX was less localized in the nucleus, and more diffusely distributed across the entire cell (Fig. 5(b)). This was probably because ionized DOX molecules were unable to permeate passively through the cell membrane effectively (Tannock, 1998) and required a longer time to localize in nucleus than do the uncharged DOX molecules that exist as a relatively large fraction at pH 7.4 (Tewes et al., 2007). This delocalized distribution of DOX at pH 6.6 prevents its interaction with the DNA of the cells, where DOX can exert its cytotoxicity, resulting in a lower cytotoxic profile compared to the case at pH 7.4.

At pH 6.6 and in the presence of α -amylase, GO₁₀₀-DEX/DOX gave the highest cytotoxic effect (IC_{50} = 3.21 μ g/mL) compared to free DOX (6.44 μ g/mL) and GO₁₀₀/DOX (9.42 μ g/mL) (Fig. 4(b)(i)). We postulated that this enhanced cytotoxicity was due to the increased cellular uptake of GO₁₀₀-DEX/DOX. This explanation is corroborated by the intracellular location result, which shows a higher fluorescence intensity of GO₁₀₀-DEX/DOX in the cytoplasm at pH 6.6 (Fig. 5(b)) compared to the weak fluorescence intensity at pH 7.4 (Fig. 5(a)). As depicted in (Fig. 6(a)), GO₁₀₀-DEX/DOX also migrated into the mitochondria, where DOX causes mitochondria dysfunction (Green and Leeuwenburgh, 2002) by inhibiting DNA topoisomerase II, which is also found in mitochondria (Chamberlain et al., 2013). This mitochondria dysfunction led to cell apoptosis and resulted in fewer mitochondrial reductases to reduce the MTT reagent in the cell viability assay, resulting in the lowest IC_{50} value. The enhanced cytotoxicity of GO₁₀₀-DEX/DOX could also come from the 48% released DOX in tumor condition as shown in release study (Fig. 3(c)(i)). These released DOX molecules, despite being possibly ionized and trapped outside the cells, could also have exerted some toxicity, similar to free DOX in these conditions. GO₁₀₀-DEX/DOX was also partially localized in lysosomes (Fig. 6(b)). Free DOX and GO₁₀₀/DOX had negligible localization in mitochondria (Chamberlain et al., 2013) and were only partially localized in lysosomes (Fig. 6) (Zeng et al., 2014).

Importantly, GO₁₀₀ and GO₁₀₀-DEX without DOX loading resulted in more than 80% cell viability even at high concentrations up to 100 μ g/mL after 48 h of treatment (Fig. 4(c)), which was similar to a previous study (Zhang et al., 2011). To carry 10 μ g/mL of DOX, only 5.6 μ g/mL

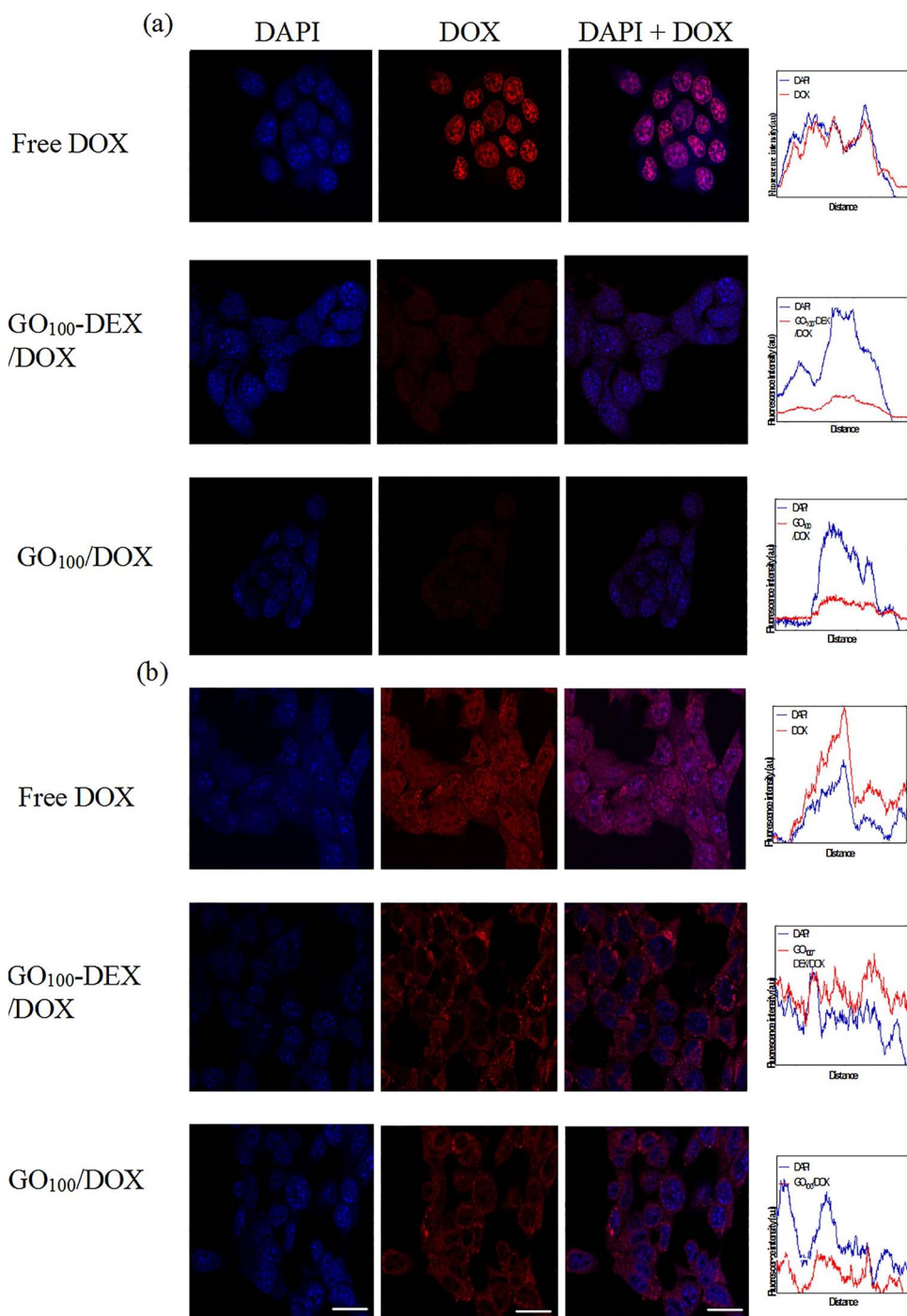


Fig. 5. Confocal images of the intracellular location of free DOX, GO₁₀₀-DEX/DOX and GO₁₀₀/DOX in 4T1 cells (a) at pH 7.4 and (b) at pH 6.6 and in the presence of α-amylase at a DOX concentration of 5 μg/mL with DAPI Tracker. Scale bar: 20 μm.

of GO₁₀₀ or GO₁₀₀-DEX was used, and they both showed negligible cytotoxic effects at this concentration.

GO₁₀₀ and GO₁₀₀-DEX are hemocompatible with a 1.3% hemolysis effect even at concentrations up to 150 μg/mL (Fig. S5(a)), which was consistent with a previous study (Liao et al., 2011). The recommended dose of DOX is 75 mg/m² (Palle et al., 2006), which is approximately 20 μg/mL of DOX in the body of a 50 kg adult. Therefore, we conducted the hemolysis assay with the DOX concentrations to 20 μg/mL. With 20 μg/mL of DOX, the hemolysis effect of GO₁₀₀/DOX and GO₁₀₀-DEX/DOX was slightly increased to approximately 2.3%, probably due to the additive lysis effect of free DOX (Cuong et al., 2011) (Fig. S5(b)). The hemolysis results of all samples were below 5% and were hence considered hemocompatible, according to biological safety standards (Liu et al., 2015), indicating that they are suitable for intravenous

administration.

3.4. Permeability of GO₁₀₀ and GO₁₀₀-DEX using a biomimetic microfluidic blood vessel model lined with a fenestrated endothelial monolayer barrier

For drug delivery to be efficacious, a drug nanocarrier must first be able to permeate through the fenestrated endothelial barrier. To our knowledge, there have only been a few studies investigating the permeability of nanocarriers through the tumor endothelial monolayer barrier (Kim et al., 2014; Pink et al., 2012; Thomas et al., 2017), and no studies specifically on GO-based nanocarriers have been published.

We employed a microfluidic device that included the principal components of biological blood vessels such as the blood vessel cavity, vascular endothelium and extracellular matrix, to mimic the tumor cell

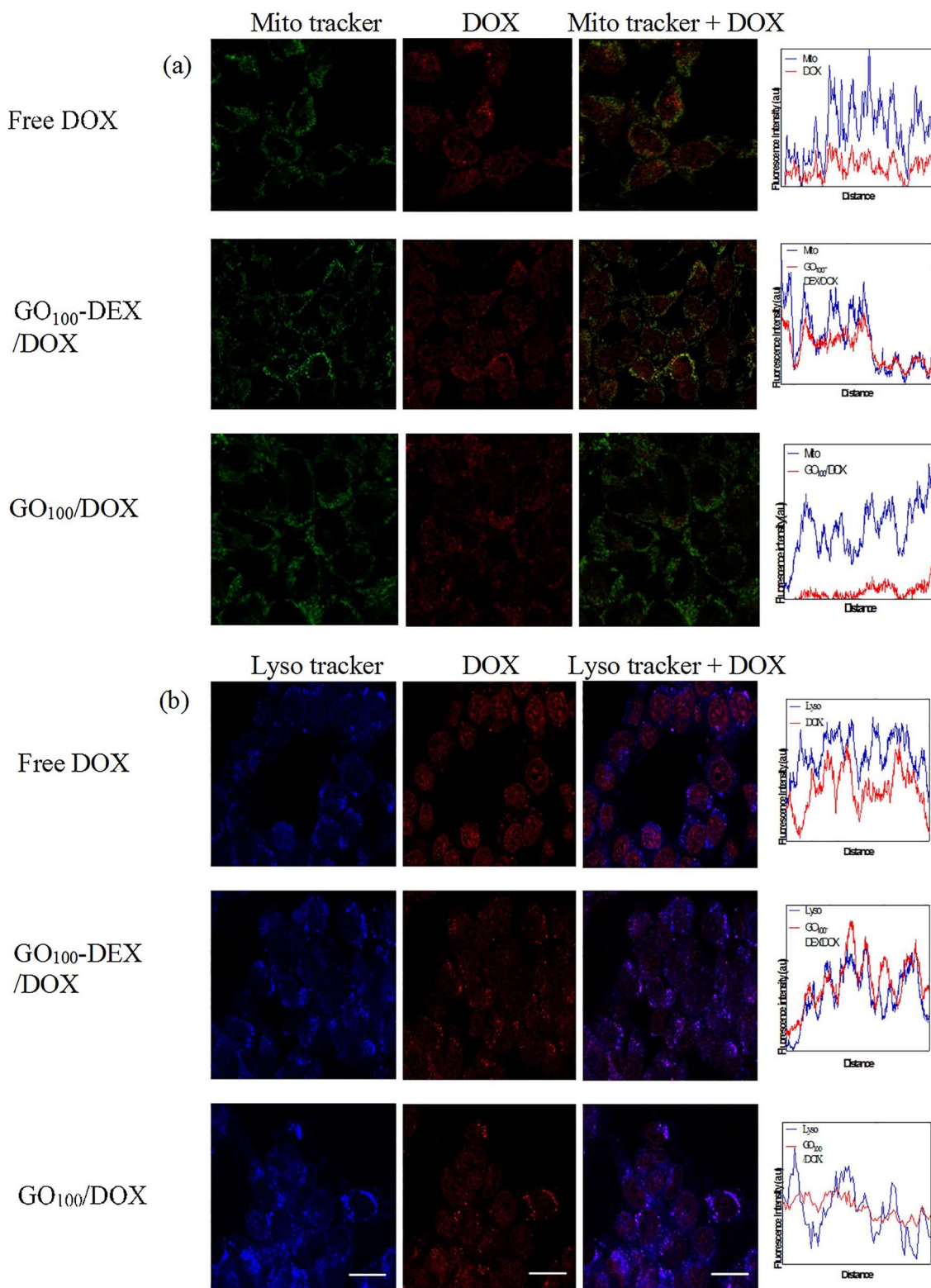


Fig. 6. Confocal images of the intracellular location of free DOX, GO₁₀₀-DEX/DOX and GO₁₀₀/DOX in 4T1 cells at pH 6.6 and in the presence of α-amylase at a DOX concentration of 5 μg/mL with (a) Mito and (b) Lyso Tracker. Scale bar: 20 μm.

microenvironment (Ho et al., 2017). In the device, nanoparticles can diffuse across the endothelial monolayer into a fibrin hydrogel that models the extracellular space. In contrast to this microfluidic model, a complicated protocol such as microsurgical implantation of a frame in anesthetized animal is required for *in vivo* work to provide a viewable imaging area (Pink et al., 2012). This surgical intervention might

induce inflammation around the viewing area that can further confound the obtained permeability results. According to Kim et al. (Kim et al., 2014), the permeability of the nanomaterials investigated using microfluidic technology is similar to the results obtained in *in vivo* experiments; thus, it considerably reduces the consumption of expensive reagents, time and labor required for *in vivo* studies (Wong et al., 2012).

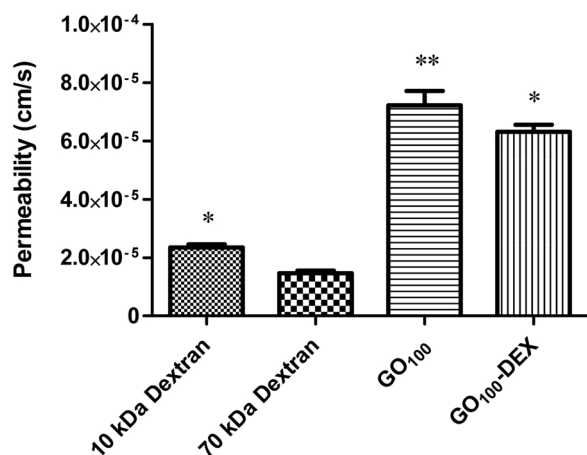


Fig. 7. Permeability results of GO₁₀₀ and GO₁₀₀-DEX compared to 10 kDa and 70 kDa dextran nanoparticles (Data represent mean \pm SEM (n = 3)).

In the microfluidic device, we seeded a monolayer of HUVECs lining the inner surface of the endothelial channel. As a functional indication of fenestration, dextrans of molecular weights 10 and 70 kDa were used to validate the endothelial barrier function in the microfluidic device. The permeability of 10 and 70 kDa dextrans was $2.35 \pm 0.11 \times 10^{-5}$ cm/s and $1.46 \pm 0.09 \times 10^{-5}$ cm/s, respectively, similar to what has been reported in previous studies (Ho et al., 2017; Zervantonakis et al., 2012). This indicates that the seeded HUVEC monolayer formed a fenestrated monolayer simulating tumor vasculature (Ho et al., 2017), which was then used as a model to evaluate the permeability of GO-based nanocarriers through the tumor vasculature to assess the efficiency of these potential nanocarriers to accumulate in tumor sites. The dextrans were also used as the comparator to study the diffusional permeability of GO₁₀₀ and GO₁₀₀-DEX as they mimic the diffusion of various macromolecular drug carriers (Pink et al., 2012) through the fenestrated vasculature.

Fig. 7 shows that the smaller the nanoparticle size, the higher the permeability of the nanoparticles through the fenestrated endothelial monolayer. For example, 10 kDa dextran had higher permeability than 70 kDa dextran, whereas GO₁₀₀ (100 nm) permeated better than GO₁₀₀-DEX did (130 nm). Compared to the dextrans, GO₁₀₀ or GO₁₀₀-DEX showed more efficient permeation through the fenestrated endothelial monolayer. The permeabilities of GO₁₀₀-DEX and GO₁₀₀ through the monolayer were 4.3- and 4.9-fold higher, respectively, than 70 kDa dextran, and 2.7- and 3.1-fold higher than 10 kDa dextran. This was probably due to the spherical dextran nanoparticles (Semyonov et al., 2014; Wasiak et al., 2016) having a reduced number of contact points when in contact with endothelial cells compared to the nonspherical GO₁₀₀ and GO₁₀₀-DEX (Blanco et al., 2015; Toy et al., 2011). Therefore, GO₁₀₀ and GO₁₀₀-DEX might have a higher tendency to marginate and adhere to the endothelial monolayer and thus have a higher permeability through the endothelial barrier. This result indicates that GO₁₀₀-DEX and GO₁₀₀ are potential drug delivery systems with better permeability than spherical nanocarriers.

There are several limitations to our study. At this stage, an *in vitro* cell model with high expression of α -amylase is not available commercially. Thus, we simulated tumor conditions by externally adding porcine α -amylase. Additionally, there is still a lack of an appropriate tumor model with high α -amylase expression for *in vivo* tests required for application of GO₁₀₀-DEX/DOX in the preclinical stage. The *in vivo* responses of the drug-loaded nanocarriers are confounded by numerous factors due to the diversity of biomolecules that exist in the human body. For example, high levels of amylase are also found in the pancreas and liver (10 unit/g of amylase activity) (Arnold and Rutter, 1963), which may result in the release of drug from GO₁₀₀-DEX in the pancreas and liver. Amylase is also released into the blood circulation of

patients with pancreatic disorders. An elevated level of α -amylase is also found in non-tumor related conditions such as abdominal lesions, pregnancy, and cardiac surgery (Dasgupta and Sepulveda, 2013). Thus, this may cause a premature release of DOX from GO₁₀₀-DEX/DOX into blood circulation, causing unwanted toxicity in normal tissues.

4. Conclusions

We synthesized an amylase-responsive GO₁₀₀-DEX nanocarrier. At acidic pH and in the presence of α -amylase, enzymatic degradation of DEX caused GO₁₀₀-DEX to release a 1.5-fold higher amount of DOX compared to GO₁₀₀. Additionally, the DEX coating led to accumulation of GO₁₀₀-DEX/DOX in the mitochondria and caused mitochondrial dysfunction via DOX. Thus, GO₁₀₀-DEX/DOX had a 2.9-fold higher cytotoxic effect than GO₁₀₀/DOX did. Under the same conditions, GO₁₀₀-DEX/DOX had a 2-fold higher cytotoxic effect compared to free DOX, whereas free DOX molecules were ionized and possibly trapped in the acidic extracellular compartment. Importantly, the permeability of GO₁₀₀-DEX and GO₁₀₀ through the fenestrated endothelial layer was at least 4.3-fold greater than the spherical 70 kDa dextrans that mimic the diffusion of various macromolecular drug carriers. The results indicate that GO₁₀₀-DEX/DOX is a promising drug nanocarrier for tumors with elevated levels of α -amylase due to the amylase-triggered DOX release and high permeability through the fenestrated endothelial barrier.

Acknowledgments

We would like to thank HIR-MoHE grants (UM.C/625/1/HIR/MOHE/MED/17 and UM.C/625/1/HIR/MOHE/MED/33) from the Ministry of Higher Education, Malaysia for financial support. SFK is a recipient of a MyPhD scholarship from the Ministry of Education, Malaysia.

Appendix A. Supplementary data

Supplementary data associated with this article can be found, in the online version, at <https://doi.org/10.1016/j.ijpharm.2017.10.045>.

References

- Arnold, M., Rutter, W.J., 1963. Liver amylase: III: synthesis by the perfused liver and secretion into the perfusion medium. *J. Biol. Chem.* 238, 2760–2765.
- Bao, H., Pan, Y., Ping, Y., Sahoo, N.G., Wu, T., Li, L., Li, J., Gan, L.H., 2011. Chitosan-functionalized graphene oxide as a nanocarrier for drug and gene delivery. *Small* 7, 1569–1578.
- Blanco, E., Shen, H., Ferrari, M., 2015. Principles of nanoparticle design for overcoming biological barriers to drug delivery. *Nat. Biotechnol.* 33, 941–951.
- Blum, A.P., Kammeyer, J.K., Rush, A.G., Callmann, C.E., Hahn, M.E., Gianneschi, N.C., 2015. Stimuli-responsive nanomaterials for biomedical applications. *J. Am. Chem. Soc.* 137, 2140–2154.
- Casadei Gardini, A., Mariotti, M., Lucchesi, A., Pini, S., Valgiusti, M., Bravaccini, S., Del Monte, A., Burgio, M.A., Marisi, G., Amadori, D., Frassinetti, G.L., 2016. Paraneoplastic lipase and amylase production in a patient with small-cell lung cancer: case report. *BMC Cancer* 16, 118–121.
- Chamberlain, G.R., Tulumello, D.V., Kelley, S.O., 2013. Targeted delivery of doxorubicin to mitochondria. *ACS Chem. Biol.* 8, 1389–1395.
- Chen, W., Yi, P., Zhang, Y., Zhang, L., Deng, Z., Zhang, Z., 2011. Composites of amino-dextran-coated Fe₃O₄ nanoparticles and graphene oxide for cellular magnetic resonance imaging. *ACS Appl. Mater. Interfaces* 3, 4085–4091.
- Cuong, N.V., Jiang, J.L., Li, Y.L., Chen, J.R., Jwo, S.C., Hsieh, M.F., 2011. Doxorubicin-loaded PEG-PCL-PEG micelle using xenograft model of nude mice: effect of multiple administration of micelle on the suppression of human breast cancer. *Cancers* 3, 61–78.
- Dasgupta, A., Sepulveda, J.L., 2013. Accurate Results in the Clinical Laboratory: a Guide to Error Detection and Correction. Elsevier.
- El-Kareh, A.W., Secomb, T.W., 2005. Two-mechanism peak concentration model for cellular pharmacodynamics of doxorubicin. *Neoplasia* 7, 705–713.
- Feng, L., Li, K., Shi, X., Gao, M., Liu, J., Liu, Z., 2014. Smart pH-responsive nanocarriers based on nano-graphene oxide for combined chemo- and photothermal therapy overcoming drug resistance. *Adv. Healthcare Mater.* 3, 1261–1271.
- Gerweck, L.E., Kozin, S.V., Stocks, S.J., 1999. The pH partition theory predicts the accumulation and toxicity of doxorubicin in normal and low-pH-adapted cells. *Br. J. Cancer* 79, 838–842.

- Green, P.S., Leeuwenburgh, C., 2002. Mitochondrial dysfunction is an early indicator of doxorubicin-induced apoptosis. *Biochim. Biophys. Acta* 1588, 94–101.
- He, D., He, X., Wang, K., Zou, Z., Yang, X., Li, X., 2014. Remote-controlled drug release from graphene oxide-capped mesoporous silica to cancer cells by photoinduced pH-jump activation. *Langmuir* 30, 7182–7189.
- Ho, Y.T., Adriani, G., Beyer, S., Nhan, P.-T., Kamm, R.D., Kah, J.C.Y., 2017. A facile method to probe the vascular permeability of nanoparticles in nanomedicine applications. *Sci. Rep.* 7, 707–719.
- Hreczuk-Hirst, D., Chicco, D., German, L., Duncan, R., 2001. Dextrins as potential carriers for drug targeting: tailored rates of dextrin degradation by introduction of pendant groups. *Int. J. Pharm.* 230, 57–66.
- Kawakita, T., Sasaki, H., Hoshihara, T., Asamoto, A., Williamson, E., 2012. Amylase-producing ovarian carcinoma: a case report and a retrospective study. *Gynecol. Oncol. Case Rep.* 2, 112–114.
- Kerr, D.J., Young, A.M., Neoptolemos, J.P., Sherman, M., Van-Geene, P., Stanley, A., Ferry, D., Dobbie, J.W., Vincke, B., Gilbert, J., el Eini, D., Dombros, N., Fountzilas, G., 1996. Prolonged intraperitoneal infusion of 5-fluorouracil using a novel carrier solution. *Br. J. Cancer* 74, 2032–2035.
- Kiew, S.F., Kiew, L.V., Lee, H.B., Imae, T., Chung, L.Y., 2016. Assessing biocompatibility of graphene oxide-based nanocarriers: a review. *J. Controlled Release* 226, 217–228.
- Kim, S., Shi, Y., Kim, J.Y., Park, K., Cheng, J.X., 2010. Overcoming the barriers in micellar drug delivery: loading efficiency, in vivo stability, and micelle-cell interaction. *Expert Opin. Drug Delivery* 7, 49–62.
- Kim, Y.K., Kim, M.H., Min, D.H., 2011. Biocompatible reduced graphene oxide prepared by using dextran as a multifunctional reducing agent. *Chem. Commun.* 47, 3195–3197.
- Kim, Y., Lobatto, M.E., Kawahara, T., Lee Chung, B., Mieszawska, A.J., Sanchez-Gaytan, B.L., Fay, F., Senders, M.L., Calcagno, C., Becraft, J., Tun Saung, M., Gordon, R.E., Stroes, E.S.G., Ma, M., Farokhzad, O.C., Fayad, Z.A., Mulder, W.J.M., Langer, R., 2014. Probing nanoparticle translocation across the permeable endothelium in experimental atherosclerosis. *Proc. Natl. Acad. Sci.* 111, 1078–1083.
- Konkena, B., Vasudevan, S., 2012. Covalently linked, water-dispersible, cyclodextrin: reduced-graphene oxide sheets. *Langmuir* 28, 12432–12437.
- Kuila, T., Bose, S., Mishra, A.K., Khanra, P., Kim, N.H., Lee, J.H., 2012. Chemical functionalization of graphene and its applications. *Prog. Mater. Sci.* 57, 1061–1105.
- Kurapati, R., Raichur, A.M., 2013. Near-infrared light-responsive graphene oxide composite multilayer capsules: a novel route for remote controlled drug delivery. *Chem. Commun.* 49, 734–736.
- Lenler-Petersen, P., Grove, A., Brock, A., Jelnes, R., 1994. alpha-amylase in resectable lung cancer. *Eur. Respir. J.* 7, 941–945.
- Liao, K.H., Lin, Y.S., Macosko, C.W., Haynes, C.L., 2011. Cytotoxicity of graphene oxide and graphene in human erythrocytes and skin fibroblasts. *ACS Appl. Mater. Interfaces* 3, 2607–2615.
- Liu, D., Auguste, D.T., 2015. Cancer targeted therapeutics: from molecules to drug delivery vehicles. *J. Controlled Release* 219, 632–643.
- Liu, D., Mori, A., Huang, L., 1992. Role of liposome size and RES blockade in controlling biodistribution and tumor uptake of GM1-containing liposomes. *Biochim. Biophys. Acta* 1104, 95–101.
- Liu, H.Y., Du, L., Zhao, Y.T., Tian, W.Q., 2015. In vitro hemocompatibility and cytotoxicity evaluation of halloysite nanotubes for biomedical application. *J. Nanomater.* 2015, 1–9.
- Mahoney, B.P., Raghunand, N., Baggett, B., Gillies, R.J., 2003. Tumor acidity, ion trapping and chemotherapeutics: I. acid pH affects the distribution of chemotherapeutic agents in vitro. *Biochem. Pharmacol.* 66, 1207–1218.
- Matthaiou, E.I., Barar, J., Sandaltzopoulos, R., Li, C., Coukos, G., Omidji, Y., 2014. Shikonin-loaded antibody-armed nanoparticles for targeted therapy of ovarian cancer. *Int. J. Nanomed.* 9, 1855–1870.
- Minami, S., Jokoji, R., Yamamoto, S., Ogata, Y., Koba, T., Futami, S., Nishijima, Y., Yaga, M., Masuhiro, K., Tsujimoto, M., Komuta, K., 2014. Amylase-producing lung cancer with a positive epidermal growth factor receptor mutation treated with gefitinib: a case report. *World J. Oncol.* 5, 41–46.
- Palle, J., Frost, B.M., Peterson, C., Gustafsson, G., Hellebostad, M., Kanerva, J., Schmiegelow, K., Lonnerholm, G., 2006. Doxorubicin pharmacokinetics is correlated to the effect of induction therapy in children with acute myeloid leukemia. *Anti-Cancer Drugs* 17, 385–392.
- Pillai, G., 2014. Nanomedicines for cancer therapy: an update of FDA approved and those under various stages of development. *SOJ Pharm. Pharm. Sci.* 1, 1–13.
- Pink, D.B.S., Schulte, W., Parseghian, M.H., Zijlstra, A., Lewis, J.D., 2012. Real-time visualization and quantitation of vascular permeability in vivo: implications for drug delivery. *PLoS One* 7, e33760–e33769.
- Predoi, D., 2007. A study on iron oxide nanoparticles coated with dextrin obtained by coprecipitation. *Digest J. Nanomater. Biostructures* 2, 169–173.
- Semyonov, D., Ramon, O., Shoham, Y., Shimoni, E., 2014. Enzymatically synthesized dextran nanoparticles and their use as carriers for nutraceuticals. *Food Funct.* 5, 2463–2474.
- Shingu, K., Ito, T., Kaneko, G., Itoh, N., 2013. Primary acinic cell carcinoma of the breast: a clinicopathological and immunohistochemical study. *Case Rep. Oncol. Med.* 2013, 1–5.
- Siriviriyun, A., Popova, M., Imae, T., Kiew, L.V., Looi, C.Y., Wong, W.F., Lee, H.B., Chung, L.Y., 2015. Preparation of graphene oxide/dendrimer hybrid carriers for delivery of doxorubicin. *Chem. Eng. J.* 281, 771–781.
- Sun, W., Zhang, N., Li, A., Zou, W., Xu, W., 2008a. Preparation and evaluation of N(3)-O-toluyll-fluorouracil-loaded liposomes. *Int. J. Pharm.* 353, 243–250.
- Sun, X., Liu, Z., Welsher, K., Robinson, J.T., Goodwin, A., Zoric, S., Dai, H., 2008b. Nanographene oxide for cellular imaging and drug delivery. *Nano Res.* 1, 203–212.
- Swietach, P., Hulikova, A., Patiar, S., Vaughan-Jones, R.D., Harris, A.L., 2012. Importance of intracellular pH in determining the uptake and efficacy of the weakly basic chemotherapeutic drug, doxorubicin. *PLoS One* 7, e35949–e35957.
- Tømmeraas, K., Vårum, K.M., Christensen, B.E., Smidsrod, O., 2001. Preparation and characterisation of oligosaccharides produced by nitrous acid depolymerisation of chitosan. *Carbohydrate Res.* 333, 137–144.
- Takeuchi, T., Fujiki, H., Kameya, T., 1981. Characterization of amylases produced by tumors. *Clin. Chem.* 27, 556–559.
- Tang, S.K.Y.W., George, M., 2010. Basic microfluidic and soft lithographic techniques. In: Yeshiahu, F., Demetri, P., Changhui, Y. (Eds.), *Optofluidics: Fundamentals, Devices, and Applications*. McGraw Hill Professional, Access Engineering.
- Tannock, I.F., 1998. Conventional cancer therapy: promise broken or promise delayed? *Lancet* 351, SII9–SIII6.
- Tewes, F., Munnier, E., Antoon, B., Ngaboni Okassa, L., Cohen-Jonathan, S., Marchais, H., Douziech-Eyrolles, L., Souce, M., Dubois, P., Chourpa, I., 2007. Comparative study of doxorubicin-loaded poly(lactide-co-glycolide) nanoparticles prepared by single and double emulsion methods. *Eur. J. Pharm. Biopharm.* 66, 488–492.
- Thomas, A., Wang, S., Sohrabi, S., Orr, C., He, R., Shi, W., Liu, Y., 2017. Characterization of vascular permeability using a biomimetic microfluidic blood vessel model. *Biomicrofluidics* 11, 024102–024117.
- Toy, R., Hayden, E., Shoup, C., Baskaran, H., Karathanasis, E., 2011. The effects of particle size, density and shape on margination of nanoparticles in microcirculation. *Nanotechnol.* 22, 115101–115109.
- Viswanathan, G., Hsu, Y.H., Voon, S.H., Imae, T., Siriviriyun, A., Lee, H.B., Kiew, L.V., Chung, L.Y., Yusa, S., 2016. A comparative study of cellular uptake and subcellular localization of doxorubicin loaded in self-assemblies of amphiphilic copolymers with pendant dendron by MDA-MB-231 human breast cancer cells. *Macromol. Biosci.* 16, 882–895.
- Wang, Y., Alewi, B.A., Wang, Q., Kurosu, M., 2012. Selective esterifications of primary alcohols in a water-containing solvent. *Org. Lett.* 14, 4910–4913.
- Wasiak, I., Kulikowska, A., Janczewska, M., Michalak, M., Cymerman, I.A., Nagalski, A., Kallinger, P., Szymanski, W.W., Ciach, T., 2016. Dextran nanoparticle synthesis and properties. *PLoS One* 11 (e0146237–e0146253).
- Weaver, C.L., LaRosa, J.M., Luo, X., Cui, X.T., 2014. Electrically controlled drug delivery from graphene oxide nanocomposite films. *ACS Nano* 8, 1834–1843.
- Wong, K.H., Chan, J.M., Kamm, R.D., Tien, J., 2012. Microfluidic models of vascular functions. *Annu. Rev. Biomed. Eng.* 14, 205–230.
- Yanagitani, N., Kaira, K., Sunaga, N., Naito, Y., Koike, Y., Ishihara, S., Ishizuka, T., Saito, R., Mori, M., 2007. Serum amylase is a sensitive tumor marker for amylase-producing small cell lung cancer? *Int. J. Clin. Oncol.* 12, 231–233.
- Yang, X., Zhang, X., Liu, Z., Ma, Y., Huang, Y., Chen, Y., 2008. High-efficiency loading and controlled release of doxorubicin hydrochloride on graphene oxide. *J. Phys. Chem. C* 112, 17554–17558.
- Zeng, X., Morgenstern, R., Nyström, A.M., 2014. Nanoparticle-directed sub-cellular localization of doxorubicin and the sensitization breast cancer cells by circumventing GST-mediated drug resistance. *Biomaterials* 35, 1227–1239.
- Zervantonakis, I.K., Hughes-Alford, S.K., Charest, J.L., Condeelis, J.S., Gertler, F.B., Kamm, R.D., 2012. Three-dimensional microfluidic model for tumor cell intravasation and endothelial barrier function. *Proc. Natl. Acad. Sci. U. S. A.* 109, 13515–13520.
- Zhang, S., Yang, K., Feng, L., Liu, Z., 2011. In vitro and in vivo behaviors of dextran functionalized graphene. *Carbon* 49, 4040–4049.